

1  
2  
3  
4  
5  
6  
7  
8  
9  
10  
11  
12  
13  
14  
15  
16  
17  
18  
19  
20  
21  
22  
23  
24  
25

**Simultaneous estimation of the soil hydraulic conductivity and the van  
Genuchten water retention parameters from an upward infiltration  
experiment**

Latorre, B., Moret-Fernández, D. \*

Estación Experimental de Aula Dei, Consejo Superior de Investigaciones Científicas  
(CSIC), P.O. Box 202, 50059 Zaragoza, Spain;

\* Corresponding author. E-mail: [david@eead.csic.es](mailto:david@eead.csic.es) Tel.: (+34) 976 71 61 40

## ABSTRACT

Accurate characterization of the saturated hydraulic conductivity,  $K_s$ , and the water retention curve,  $\theta(h)$ , are crucial to correctly model the water flow into the soil. This paper presents a new laboratory method to simultaneously estimate  $K_s$  and  $\alpha$  and  $n$  parameters of the van Genuchten (1980)  $\theta(h)$  from the inverse analysis of an upward infiltration curve measured in a 5-cm high soil column. The method was evaluated on synthetic 1D infiltration curves generated for a theoretical loamy sand, loam and clay soil. In a first step, the  $K_s$ - $\alpha$ ,  $n$ - $K_s$  and  $\alpha$ - $n$  error maps were evaluated, using in each case the remaining theoretical hydraulic parameter. The influence of the soil initial condition on the inverse analysis was also studied. Next, an optimization method was presented and tested on eight theoretical soils (from loamy sand to clay). The method was subsequently applied to experimental infiltration curves measured on five sieved soils (from sand to clay) packed in 5-cm high and diameter cylinders. The  $K_s$ ,  $\alpha$  and  $n$  values estimated from the inverse analysis of the experimental curves were compared to those measured by Darcy and the pressure cell method (PC). The initial soil tension,  $h_i$ , which had an important influence on the optimization, was fixed to  $-6.0 \cdot 10^5$  cm. A unique minimum was observed in all  $K_s$ - $\alpha$ ,  $n$ - $K_s$  and  $\alpha$ - $n$  error maps generated for the synthetic loamy sand, loam and clay soils. The optimization method resulted robust and allowed accurate estimates of the actual hydraulic parameters. A close to one relationship ( $R^2 = 0.99$ ) was observed between the theoretical  $K_s$ ,  $\alpha$  and  $n$  and the corresponding values obtained with the inverse analysis. Regarding to the experimental soils, significant relationships close to one were obtained between  $K_s$  and  $n$  ( $R^2 > 0.98$ ) estimated from inverse analysis and those measured with Darcy and PC. A non-significant relationship with slope away from one was found for  $\alpha$ .

**Keywords:** Soil Hydraulic Properties; Sorptivity; Inverse Analysis; Richard's Model.

## 1. INTRODUCTION

Characterization of the hydraulic conductivity,  $K$ , and the water retention curve,  $\theta(h)$ , is crucial to determine the water flow in the vadose zone.  $K$  is a measure of the soil ability to transmit water when soil is submitted to a hydraulic head gradient. This parameter depends on the soil water content, the pressure head and the flux across the boundary of a soil compartment (Dane and Hopmans 2002). The soil water retention curve describes the relationship between the volumetric water content,  $\theta$  [ $\text{L}^3 \text{L}^{-3}$ ], and the matric potential,  $h$  [L].  $\theta(h)$  depends upon the particle-size distribution, which determines the soil texture, and the arrangement of the solid particles, which refers to the soil structure (Dane and Hopmans, 2002). One of the most common functions used to describe  $\theta(h)$  is the unimodal van Genuchten (1980) model, which is defined by the saturated ( $\theta_s$ ) and residual ( $\theta_r$ ) volumetric water content and the empirical  $\alpha$  and  $n$  factors. An additional  $m$  parameter, commonly defined as  $m = 1 - \left(\frac{1}{n}\right)$ , is also employed.  $\theta_r$  is defined as the water content for which the gradient  $d\theta/dh$  becomes zero (excluding the region near  $\theta_s$  which also has a zero gradient),  $n$  [-] is the slope of  $\theta(h)$  and is related to pore-size distribution, and  $\alpha$  [ $\text{L}^{-1}$ ] is a scale factor that defines the shape of  $\theta(h)$  near  $\theta_s$ .

The saturated hydraulic conductivity,  $K_s$ , can be measured with either the constant head or the falling-head method (Klute and Dirksen, 1986). The reference laboratory method used to determine  $\theta(h)$  is the pressure extractor (Klute, 1986). Although this technique has been improved by incorporating alternative methods to determine  $\theta$  (Jones et al., 2005; Moret-Fernández et al., 2012), the long time needed to conclude a

measurement together with its limitations on fine textured soils (Solone et al., 2012) can restrict its use.

Other family of methods to estimate  $K$  and  $\theta(h)$  are based on the inverse numerical analysis of Richard's transient water flows. The main advantage of these techniques is the simultaneous estimation of  $\theta(h)$  and  $K(h)$ . To date, four different methods based on the inverse analysis of a transient water flow are available: evaporation and horizontal-, downward- and upward-infiltration processes. The evaporation method is based on the Wind (1968) formulation, where soil tension is measured within a vertical soil column as water evaporates from its surface using tensiometers installed at multiple depths, and water content and flux are determined by weighing the column. In more recent studies, Wind's method has been modified and simplified (e.g., Schindler, 1980; Simunek et al., 1996; Schindler and Müller, 2006; Schindler et al., 2010; Masaoka and Kosugi, 2018). The horizontal infiltration method is based on the Shao and Horton (1998) procedure, where the saturated hydraulic conductivity is measured by Darcy, and  $\alpha$  and  $n$  van Genuchten (1980) parameters are estimated with an integral method that solves the problem of water absorption into a horizontal soil column. To this end, a soil column inserted in a 20 cm-length transparent cylinder should be used. The downward infiltration method analyzes cumulative infiltration rates measured with a disc infiltrometer at several consecutive tensions (Simunek and van Genuchten, 1997). The combination of multiple tension cumulative infiltration data with measured initial and final water contents yields unique solutions of the inverse problem for the unknown parameters. This method has been successfully used in several studies, such as Ramos et al. (2006), Caldwell et al. (2013) or Rashid et al. (2015), among others.

Up to date, different laboratory upward infiltration methods have been developed. Hudson et al. (1996) estimated  $\theta(h)$  and  $K(h)$  from the inverse analysis of an upward

flow using a constant flux of water at the bottom of the soil sample. Young et al. (2002) combined the water cumulative flux and the soil pressure head measured by two tensiometers installed along a 15-cm-long soil column. Although this technique gave satisfactory results, the long soil columns used in the experiment together the use of tensiometers may prevent its use in undisturbed soil samples. Moret-Fernández et al. (2016b) developed a method where  $K_s$  was calculated according to the Darcy's law and the  $\theta(h)$  parameters were estimated from the inverse analysis of a multiple tension water absorption curve. Although the method proved effective, the high negative pressure head needed at the beginning of the experiment restricted its use to sieved soils. Peña-Sancho et al. (2017) estimated the soil hydraulic properties from a capillary wetting process at saturation followed by an overpressure step and an evaporation process. In this case,  $K_s$  was calculated by Darcy and the hysteresis phenomenon was introduced using an empirical model. Finally, Moret-Fernández and Latorre (2017) estimated the  $\theta(h)$  parameters from  $K_s$  measured by Darcy and the sorptivity,  $S$ , and  $\beta$  parameter (Haverkamp et al., 1994). In this case  $S$  and  $\beta$  were estimated from the inverse analysis of an upward infiltration curve. Although this technique was satisfactorily validated on 5-cm high theoretical and experimental soils, the employed formulation restricted its use to soils ranged from sand to silt textural classes (Lassabatere et al., 2009).

Although all above cited references show that the upward infiltration is an effective process to estimate  $\theta(h)$  and  $K(h)$ , further efforts are needed to develop an alternative method that allows simultaneous estimate of all hydraulic properties, in any kind of soil and using short soil columns. This work presents a new method to determine  $K_s$ ,  $\alpha$  and  $n$  from the inverse analysis of an upward infiltration curve measured on a 5-cm high soil column. The method was firstly evaluated with a global analysis applied on upward infiltration curves generated by HYDRUS-1D for a loamy sand, loam and clay soil. The

influence of the initial soil pressure head on the inverse analysis was also studied. Next, an optimization method was proposed and tested on eight theoretical soils. The method was finally applied on experimental infiltration curves measured on different sieved soils of known hydraulic properties.

## 2. MATERIAL AND METHODS

### 2.1. Theory

The one-dimensional water flow equation in a variably saturated rigid porous medium is defined by the Richards model

$$\frac{\partial \theta}{\partial t} = \frac{\partial}{\partial z} \left( K \frac{\partial h}{\partial z} + K \right) \quad (1)$$

where  $\theta$  is the volumetric soil water content [ $L^3 L^{-3}$ ],  $t$  is time [T],  $z$  is a vertical coordinate [L], positive upward,  $h$  is the soil-water pressure head [L] and  $K$  is the hydraulic conductivity [ $L T^{-1}$ ].

The soil hydraulic functions can be described by the van Genuchten-Mualem functions (van Genuchten, 1980)

$$S_e(h) = \frac{\theta(h) - \theta_r}{\theta_s - \theta_r} = \left[ 1 + (\alpha h)^n \right]^{-m} \quad (2)$$

$$K(S_e) = K_s S_e^l \left[ 1 - \left( 1 - S_e^{1/m} \right)^m \right]^2 \quad (3)$$

where  $S_e$  is the effective saturation [-],  $\theta_s$  and  $\theta_r$  are the saturated and residual water content, respectively,  $\alpha$  [ $L^{-1}$ ] and  $n$  [-] are shape parameters,  $m=1-1/n$ ,  $l$  is a pore-connectivity parameter and  $K_s$  is the saturated hydraulic conductivity. Similar to defined

by Simunek et al. (1996, 1998), Simunek and van Genuchten et al. (1997) and Young et al. (2002), among others,  $l$  was fixed to 0.5. Because  $\theta_r$  and  $\theta_s$  can be easily measured at the beginning and the end of the experiment, respectively, the hydraulic characteristics defined by Eq. (2) and (3) were reduced to three unknown parameters:  $\alpha$ ,  $n$  and  $K_s$ . In our case, these equations represent the wetting branch of the unsaturated hydraulic properties.

The soil sorptivity,  $S$ , [ $L T^{-0.5}$ ] is defined as the capacity of a porous medium to absorb liquid by capillarity (Philip, 1957).  $S$ , expressed as function of the van Genuchten (1980) parameters, results (Moret-Fernández, et al., 2017a)

$$S^2 = \frac{(1-m)K_s}{\alpha m(\theta_s - \theta_r)} \int_{\theta_i}^{\theta_s} [\theta_s + \theta - 2\theta_i] S_e^{\frac{1}{2}-\frac{1}{m}} \left[ \left(1 - S_e^{\frac{1}{m}}\right)^{-m} + \left(1 - S_e^{\frac{1}{m}}\right)^m - 2 \right] d\theta \quad (4)$$

where  $\theta_i$  is the initial water content. The soil sorptivity expressed as function of an upward infiltration curve,  $S^*$ , can be expressed as (Moret-Fernández, et al., 2017a)

$$I = S^* \sqrt{t} - Ct \quad (5)$$

where  $I$  [L] is the cumulative upward infiltration and  $C$  is a constant that is related to the soil hydraulic conductivity (Minasny and McBratney, 2000). This equation is only valid for short-medium infiltration times.

## 2.2. Numerical simulations

The synthetic upward infiltration data was generated using the HYDRUS-1D software (Simunek et al., 1996). The method was tested on eight theoretical soils (Carsel and Parrish, 1988) ranged from loamy sand to clay soil textural classes (Table 1).

A 5 cm-high soil column was discretized with a 1-D mesh of 1000 cells. Previous conducted numerical analysis demonstrated that, under this discretization, the solution was grid independent. The initial time step in the simulation, which value depended on the total infiltration time, varied from  $10^{-5}$  s to 0.025 s for sand to clay, respectively. The tension at the base of the soil column was 0 cm. The evaporation rate was considered null and atmospheric conditions with a maximal tension of 0 cm was imposed at the top boundary. Time zero corresponded to the beginning of the upward infiltration process, and the simulation finished when the wetting front arrived to the soil surface.

### 2.3. Inverse analysis

The  $\alpha$ ,  $n$  and  $K_s$  parameters were calculated by minimizing an objective function,  $\Phi(\alpha, n, K_s)$ , that represents the difference between HYDRUS-1D simulated curves and synthetic or experimental infiltration data

$$\Phi = \sqrt{\frac{\sum_1^N (I_e(t_i) - I_s(t_i))^2}{N}} \quad (6)$$

where  $N$  is the number of measured  $I$  values,  $I_e(t_i)$  and  $I_s(t_i)$  are specific measurements at time  $t_i$ . The values of the objective function were initially summarized as contours lines in the  $K_s$ - $n$ ,  $\alpha$ - $n$ , and  $K_s$ - $\alpha$  error maps, given in each plane the remaining theoretical hydraulic parameter.  $K_s$ ,  $\alpha$  and  $n$  values ranged from  $10^{-5}$  to  $10^{-2}$  cm s<sup>-1</sup>, 0.01 to 0.1 cm<sup>-1</sup>, and 1.01 to 3.0, respectively, and  $K_s$  and  $\alpha$  were logarithmically sampled. The parameter combination for each response surface were calculated on a rectangular grid. Each parameter was discretized into 100 points, resulting in 10000 grid points for each



response surface. These error maps were generated for a theoretical loamy sand, loam and clay soil.

The influence of the initial pressure head ( $h_i$ ) on the global optimization was studied on a synthetic loam soil. Two different initial soil tensions were compared:  $-1.0 \cdot 10^3$ ,  $-6.0 \cdot 10^5$  cm. These  $h_i$  correspond to a soil sample in equilibrium with an atmosphere at 20 °C and relatively humidity of  $\approx 100$  and 60%, respectively (RILEM, 1980).

Experimental data is subject to several sources of uncertainty (i.e. water level drop in the water reservoir, initial and final water content, etc.). Only the experimental error corresponding to the water level measurement in the water reservoir was considered. A preliminary experiment performed with a  $\pm 72$  cm pressure transducer installed in a 1.9 cm-diameter water reservoir and connected to a 5 cm-diameter soil cylinder resulted in a soil water infiltration measurement uncertainty of  $\pm 0.02$  mm. The change of the objective function (Eq. 5) associated to the uncertainty source was first calculated and superimposed on the response surfaces in the form of a contour line (0.02 mm).

The soil sorptivity defined in the cumulative upward infiltration curve (Eq. 5),  $S^*$ , was calculated by applying an objective function that calculates the squared difference between numerically generated and predicted cumulative infiltration curves, where we set it to be minimized based the target parameters ( $S, C$ ).

## 2.4. Optimization method

Previous studies on upward infiltration processes (Moret-Fernández et al., 2016, Peña-Sancho et al., 2017) have shown ill-conditioned error maps with long ellipsoid

contours or elongated valleys. Given that a brute-force search is time-consuming (Horst and Romeijn, 2002), local optimization methods should be employed. First-order optimization methods, like gradient descent, oscillate quickly across the valley but move slowly along the valley floor. This results in extremely low convergence. Newton methods overcome this problem relying on the two first derivatives of the function: the gradient and the Hessian (Avriel, 2003). In the case of the Richards equation, the gradient function is not given and it is computed numerically. Any noise in this calculation, such as that introduced by numerical simulation, amplifies when the Hessian is inverted and introduces noise and instabilities.

Random search (RS) is a family of stochastic optimization methods that do not require the gradient of the function to be optimized (Brooks, 1958). The basic RS algorithm can be described as follows:

1. Initialize  $x$  with a random position in parameter-space.
2. Until a termination criterion is met, repeat the following:
  1. Sample a new position  $y$ , moving  $x$  in a random direction a given fixed step
  2. If  $f(y) < f(x)$  then move to the new position by setting  $x = y$

Adaptive Step Size Random Search (ASSRS) (Schumer and Steiglitz, 1968) attempts to heuristically adapt the step size to improve the performance of the search. Though ASSRS is quite effective in reducing the objective function during the initial search phases, the average linear convergence rate is rather slow for more precise solutions. In order to obtain accurate estimations, deterministic optimization techniques are needed (Haiping, 1996).

In this work, ASSRS was combined with a gradient search method. In each iteration, a random direction is first proposed and explored. Subsequently a deterministic direction is computed based on the linear regression of the last five successfully points and is also explored. In both cases, an initial step size of  $10^{-3}$  is considered which is incremented exponentially while the error is reduced. The explored variables were transformed to the (0,1) interval using the following extreme values:  $K = [10^{-6}, 10^{-2}]$  cm  $s^{-1}$ ,  $\alpha = [10^{-3}, 0.5]$   $cm^{-1}$ ,  $n = [1.0, 3.5]$  and considering logarithmic transformations in the case of  $K$  and  $\alpha$ . This transformation simplifies calculations, guarantees the same properties in all explored directions and allows to accurately explore physical variables covering several orders of magnitude.

## 2.5. Experimental validation

The experimental upward infiltration curves were measured with a sorptivimeter device (Moret-Fernández et al., 2017a). This consists of a saturated perforated base 5 cm-internal diameter (i.d.) that accommodates a stainless steel cylinder (5 cm-i.d. x 5 cm-high) that contains the soil sample. The bottom of the perforated base is connected to a Mariotte water supply reservoir (30 cm high, 1.9 cm-i.d). A  $\pm 7.2$  kPa differential pressure transducer (Microswitch; Honeywell International Inc.) connected to a datalogger (CR1000; Campbell Scientist, Inc., Logan, UT, USA) was installed at the bottom of the water supply reservoir. The time interval of the water level measurements was 1 s. To minimize the water losses by evaporation, the surface of the soil column was covered with a lid. More details of the sorptivimeter can be found in Moret-Fernández et al. (2017a).

The upward infiltration method was applied on five 2-mm sieved soils with textural classes ranging from sand to clay (Table 2). The sieved material was initially stored at  $\approx 20\text{ }^{\circ}\text{C}$  and  $\approx 30\%$  of relative humidity during several months. Since the soil is in equilibrium with the air in the chamber, the soil tension corresponding to this atmospheric condition is  $-1.6 \cdot 10^6\text{ cm}$  (RILEM, 1980). The soils were next homogeneously packed in 5-cm high and diameter cylinders and weighted. To this end, the sieved soil was poured in by hand and gently tapped in small incremental steps to achieve a uniform bulk density. This initial weight defined the residual gravimetric water content. Next, the cylinders were stored during several months at a temperature of  $\approx 20\text{ }^{\circ}\text{C}$  and relative humidity of  $\approx 60\%$ , which corresponds to a soil pressure head of  $-6.0 \cdot 10^5\text{ cm}$  (RILEM, 1980). The upward infiltration started when the cylinder containing the soil was placed on the sorptivimeter, and finished when the wetting front arrived at the soil surface. At this time, the soil sample was saturated by raising the air inlet tube of the Mariotte reservoir to the soil surface. Once the soil sample was saturated, the core was disassembled, weighted, dried at  $105\text{ }^{\circ}\text{C}$  during 24 h, and weighted again. Soils with high gypsum content (Table 1) were dried at  $50\text{ }^{\circ}\text{C}$  during 48 h (Moret-Fernández et al. 2016b). The soil bulk density ( $\rho_b$ ) was calculated as the product between the core volume and the dry-weight of the soil.  $\theta_s$  and  $\theta_r$  were calculated as the product between  $\rho_b$  and the corresponding gravimetric data. Once  $\theta_s$  and  $\theta_r$  calculated,  $K_s$  and  $\alpha$  and  $n$  were finally estimated by applying the optimization method to the corresponding upward infiltration curves.

The  $K_s$  and  $\alpha$  and  $n$  parameters estimated from the inverse analysis were compared with those calculated by Darcy and the pressure cell, PC, method (Moret-Fernández et al. 2012), respectively. The volumetric water content in the PC was measured by TDR

at air-dried soil conditions, which corresponds to a pressure head ( $h$ ) of approximately – 1.6 MPa, at soil water saturation and at pressure heads of –0.5, –1.5, –3, –10 and –50 kPa. In this case,  $\theta_r$  and  $\theta_{sat}$  corresponded to the air-dried and saturated water content measured by TDR, respectively. The measured pairs of  $\theta$  and  $h$  values were numerically fitted to the van Genuchten (1980) model (Eq. 2). To this end,  $\theta_{sat}$  and  $\theta_r$  were considered as known values, and  $\alpha$  and  $n$  were estimated by minimizing an objective function that represents the difference between model and experimental data (Moret-Fernández et al., 2017b). The saturated hydraulic conductivity was estimated by the Darcy’s law. Because the inverse analysis of upward infiltration curves and PC methods define the opposite branches of the water retention curve,  $\alpha$  values obtained with PC were converted to the wetting branch of the water retention curve using the Gebrenegus and Ghezzehei (2011) hysteresis index.

### 3. RESULTS AND DISCUSSION

The analysis of the results obtained on the synthetic loam soil shows that  $h_i$  had an important influence on the error maps (Fig. 1). When the initial tension is located in the transition zone of the water retention curve (i.e.  $-1.0 \cdot 10^3$  cm) (Fig. 1), small variations of  $n$  and  $\alpha$  produce large changes in the initial soil water content. This translates into error maps with a focused minimum. Although the contour lines of the error maps tend to length when initial tension is shifted to the flat zone of the water retention curve (i.e.  $6.0 \cdot 10^{-5}$ ), the minimum is still preserved (Fig. 1). These results indicate that very extremely negative  $h_i$  should not be employed. Overall, initial soil tension of  $-10^3$  cm could be experimentally obtained with a pressure extractor. However, we discard this technique because the pressure plates method is not consistent in fine soils (Solone et al., 2012), and it has little effectiveness in long cores (i.e. 5 cm high), where the very

long draining time needed to stabilize the water content into the soil core can restrict its use. On the other hand, the soil water draining process within the pressure plates, which can alter the soil structure by collapsing the more unstable soil macrostructure (Moret-Fernández et al. 2016a), can modify the actual soil hydraulic properties. In any case, the use of a pressure extractor would be only recommendable in very stable and permeable soils. Alternatively, suitable  $h_i$  can be achieved by placing the soil samples in equilibrium in an atmosphere with high relative humidity. For instance, a pressure head of  $-6.0 \cdot 10^5$  cm can be obtained when a soil sample is stored at 20 °C and 60% relative humidity (RILEM, 1980). Given that these atmospheric conditions are not difficult to accomplish, the initial tension considered from now on, both in the theoretical and experimental analysis, will be fixed to  $-6.0 \cdot 10^5$  cm.

Upward infiltration curves were longer in finer soils (Fig. 2). The  $\alpha$ - $n$ ,  $K_s$ - $n$  and  $K_s$ - $\alpha$  response surfaces calculated for the loamy sand, loam and clay soils showed, in all cases, an unique minimum (Fig. 2). These results indicate that  $K_s$ ,  $\alpha$  and  $n$  can be estimated from the inverse analysis of a single upward infiltration curve. However, the shapes of the error map varied depending on the soil type. For instance, the vertical and elongated  $\alpha$ - $n$  and  $K_s$ - $n$  error maps observed in loamy sand makes that small changes in  $\alpha$  or  $K_s$  promoted important variations of  $n$ . This can be related to the commonly abrupt  $\theta(h)$  shapes observed in coarse soils, where small changes of the water retention slope make important variations in  $n$ . An opposite behavior was observed in clay, where the more horizontal  $\alpha$ - $n$  and  $K_s$ - $n$  error maps made that minor changes in  $n$  promoted large variations of  $\alpha$  and  $K$ . This dependence can be related to the flatter  $\theta(h)$  shapes observed in fine soils, where large changes of  $\alpha$  may induce small variations in the  $\theta(h)$  slope. An intermediate behavior was observed in the loam soil (Fig. 2). These results, however, contrast with those obtained by Moret-Fernández et al. (2016a) and Peña-Sancho et al.

(2017), where error maps calculated from the inverse analysis of an upward infiltration curve did not show an absolute minimum. These differences are explained because the soil initial condition used in those works was fixed in volumetric water content instead on pressure head. Under these circumstances,  $\theta_i$  was set close to the measured  $\theta_r$ , and  $h_i$  resulted free and dependent of  $\alpha$  and  $n$ . These results indicate the initial soil tension is a key physical parameter in the capillarity processes. Moreover, the differences regarding to the above cited works could be also explained because of the steady-state phase at the end of the upward infiltration was not included in the inverse analysis. This assumption suggests that the measurement of the steady-state section is crucial to optimize the soil hydraulic properties.

Given the ill-conditioning of the error maps, the hydraulic parameters were estimated using an stochastic optimization method. The procedure was based on the ASSRS method, introducing preferential directions in the random search to increase convergence rate at the final stage of the optimization. The last ten successful points explored by the ASSRS method were linearized to approximate the direction that leads to the minimum. The satisfactory convergences of the optimization method in a loam soil, starting from four different initial values, indicate the proposed method allows accurate estimates of  $\alpha$ ,  $n$  and  $K_s$ , independently of the initial value (Fig. 3). A robust relationship (Fig. 4a) ( $R^2 > 0.99$ ) was observed between the theoretical  $K_s$ ,  $\alpha$  and  $n$  and the corresponding optimized values (Table 1). In all cases,  $\Phi$  (Eq. 6) was lower than  $5.0 \cdot 10^{-4}$  cm. The weak dispersion found in  $K_s$  and  $\alpha$  on clay can be related to the quasi-horizontal  $\alpha$ - $n$  and  $K_s$ - $n$  error maps observed in this soil (Fig. 2), where small variations in  $n$  can make large changes in  $\alpha$  and  $K$ . An also robust relationship ( $R^2 > 0.99$ ) was found between the theoretical hydraulic properties and the intermediate values for a 0.02 mm error (Fig.4b), which corresponds with the experimental threshold error

defined in Section 2.3. These results indicate that the proposed optimization can be satisfactorily applied to any kind of soil. The optimization, however, could be accelerated if initial hydraulic parameters ( $K_s'$ ,  $\alpha'$  and  $n'$ ) close to the actual values were selected. For instance, these initial values could be obtained from the  $K_s(S)$ ,  $\alpha(S)$  and  $n(S)$  regressions (Fig. 5), where  $S$  is integrated between  $\theta_s$  and  $\theta_i$  (Eq. 4). This relationship will be subsequently used to estimate  $K_s'$ ,  $\alpha'$  and  $n'$  (Table 1) from  $S^*$  (Eq. 5).

The  $S^*$  values estimated from the experimental infiltration curves (Eq. 5), together with the corresponding  $K_s'$ ,  $\alpha'$  and  $n'$  are summarized in Table 2. Overall, good fittings were observed between the measured upward infiltration curves and the optimized ones (Table 2). For instance, Figure 6 compares the experimental vs. the best optimized curve, as well as the iterations followed by the optimization method applied to the experimental clay soil. A robust and significant relationship, with slope close to one and an average dispersion of 0.4% (Fig. 7), was observed between  $n$  measured with PC and the corresponding values estimated from the inverse analysis of the experimental infiltration curves (Fig. 7). This strong relationship could be associated to the fact that  $n$  is more related to the soil textural characteristics (Jirku et al., 2013), and hence, less affected by the influence of the wetting-drainage process on the soil structure (Moret-Fernández et al., 2016a). Similar results were obtained by Moret-Fernández et al. (2016b) and Moret-Fernández and Latorre (2017) with comparable upward infiltration methods. An also significant relationship, with slope close to one, was observed between the optimized  $K_s$  and the corresponding value obtained by Darcy. In this case,  $\log(K_s)$  measured by Darcy was 2.5% higher than that estimated by the inverse analysis. A no-statistically significant relationship, with a slope away from the 1:1 line, was observed between  $\alpha$  estimated with PC and that obtained with the infiltration method.



Similar results were obtained by Moret-Fernández and Latorre (2017) with a comparable upward infiltration method. This behavior could be explained by the different wetting processes used in both methods (Moret-Fernández and Latorre, 2017), which may modify the contact angle of water with the soil particles, the amount of air entrapped in the pores, or the interconnection in the pore network (Bachmann and van der Ploeg, 2002; Maqsoud et al., 2004). Other explanation could be found in the empirical Gebrenegus and Ghezzehei (2011) hysteresis model, that could give an inaccurate description of  $\alpha$  for a wetting process. An indirect confirmation for this hypothesis is given by the good correlation found in  $K_s$  and  $n$ , which are less affected by the hysteresis. A robust and significant relationship with slope close to one (Fig. 8) was observed between  $S$  calculated by applying the optimized  $\alpha$ ,  $n$  and  $K_s$  values to Eq.(4) and the corresponding  $S^*$  (Eq. 5) estimated from the upward infiltration curve. This satisfactory relationship corroborates the robustness of the inverse analysis.

## CONCLUSIONS

This work demonstrates that  $K_s$ ,  $\alpha$  and  $n$  can be estimated from the inverse analysis of a single upward infiltration curve measured on a 5-cm high cylinder, when the initial soil tension is fixed to  $-6.0 \cdot 10^5$  cm. A robust and efficient optimization method was proposed and satisfactorily validated on theoretical and experimental sieved soils contained in 5-cm high cylinders. Unlike previous methods, this new technique is simple, inexpensive, fast to implement, allows simultaneous estimates of all hydraulic parameters, can be applied to any kind of sieved soils and on the 5-cm high cores commonly employed for soil bulk density determination. However, new efforts should

be done to test the method on heterogeneous and undisturbed soil samples, and to study the influence of the core length on the hydraulic properties estimation.

## Acknowledgments

The authors are grateful to the Área de Informática Científica de la SGAI (CSIC) for their technical support in the numerical analysis and to Dra. M.V. López, R. Gracia and M.J. Salvador for they help in some laboratory tasks. The authors are also grateful to Dr. K. Seki and Dr. R. Angulo-Jaramillo for their advices in some theoretical aspects of the paper.

## References

- Avriel, M. Nonlinear Programming: Analysis and Methods. Englewood Cliffs (N.J.). Prentice-Hall, 2003.
- Bachmann, J., van der Ploeg, R.R., 2002. A review on recent developments in soil water retention theory: interfacial tension and temperature effects. Journal of Plant Nutrition and Soil Science 165, 468–478.
- Brooks, S.H., 1958. A Discussion of Random Methods for Seeking Maxima. Operations Research 6, 244-251.
- Caldwell, T.G., Wohling, T., Young, M.H., Boyle, D.P., McDonald, E.V. 2013. Characterizing disturbed desert soils using multiobjective parameter optimization. Vadose Zone Journal 12 (1).

425 Carsel, R.F., Parrish, R.S., 1988. Developing joint probability distributions of soil water  
426 retention characteristics. *Water Resources Research*. 24, 755–769.

427 Dane J.H., Hopmans J.W. 2002. Water retention and storage. In *Methods of Soil*  
428 *Analysis*. Part. 4, Dane JH and Topp GC (editors). SSSA Book Series No. 5.  
429 Soil Science Society of America, Madison, WI.

430 Gebrenegus, T., Ghezzehei, T.A., 2011. An index for degree of hysteresis in water  
431 retention. *Soil Science Society of America Journal* 75, 2122–2127

432 Haverkamp, R., Ross, P.J., Smettem, K.R.J., Parlange, J.Y. 1994. Three dimensional  
433 analysis of infiltration from the disc infiltrometer. Part 2. Physically based  
434 infiltration equation. *Water Resources Research* 30, 2931-2935.

435 Haiping, Z., Yamada K. 1996. Estimation for urban runoff quality modeling. *Water*  
436 *Science and Technology*. 34, 49-54.

437 Horst, R., Romeijn, H.E. (Eds.), 2002. *Handbook of Global Optimization*, vol. 2.  
438 Springer Science & Business Media.

439 Hudson, D.B., Wierenga, P.J., Hills, R.G., 1996. Unsaturated hydraulic properties from  
440 upward flow into soil cores. *Soil Science Society of America Journal* 60, 388–  
441 396.

442 Jirku, V., Kodesová, R., Nikodem, A., Mühlhanslová, M., Zigová, A., 2013. Temporal  
443 variability of structure and hydraulic properties of topsoil of three soil types.  
444 *Geoderma* 204, 43–58.

445 Jones, S.B., Mace, R.W., Or, D., 2005. A time domain reflectometry coaxial cell for  
 446 manipulation and monitoring of water content and electrical conductivity in  
 447 variable saturated porous media. *Vadose Zone Journal* 4, 977–982.

448 Klute, A. 1986. Water retention curve: laboratory methods. In: Klute, A. (Ed.), *Methods*  
 449 *of Soil Analysis. Part 1. SSSA Book Series No. 9. Soil Science Society of*  
 450 *America, Madison WI.*

451 Klute, A. and Dirksen, C. 1986. Hydraulic conductivity and diffusivity: Laboratory  
 452 methods. In: Klute, A. Ed., *Methods of Soil Analysis - Part 1 - Physical and*  
 453 *Mineralogical Methods, American Society of Agronomy, Madison, 687-734.*

454 Lassabatere, L., Angulo-Jaramillo, R., Soria-Ugalde, J.M., Simunek, J., Haverkamp, R.,  
 455 2009. Numerical evaluation of a set of analytical infiltration equations. *Water*  
 456 *Resources Research* 45. <http://dx.doi.org/10.1029/2009WR007941>.

457 Latorre, B., Peña, C., Lassabatere L., Angulo-Jaramillo R., Moret-Fernández, D. 2015.  
 458 Estimate of soil hydraulic properties from disc infiltrometer three-dimensional  
 459 infiltration curve. Numerical analysis and field application. *Journal of Hydrology*  
 460 57, 1-12.

461 Maqsoud, A., Bussiere, B., Mbonimpa, M., Aubertin, M., 2004. Hysteresis effects on  
 462 the water retention curve: a comparison between laboratory results and predictive  
 463 models. In: *Proc. 57th Can. Geotech. Conf. and the 5th joint CGS-IAH Conf.,*  
 464 *Quebec City. 24–27 October. The Canadian Geotechnical Soc., Richmond, BC,*  
 465 *pp. 8–15.*

466 Masaoka, N., Kosugi, K. 2018. Improved evaporation method for the measurement of  
 467 the hydraulic conductivity of unsaturated soil in the wet range. *Journal of*  
 468 *Hydrology* 563, 242–250.

469 Minasny, B., McBratney, A.B. 2000. Estimation of sorptivity from disc-permeameter  
 470 measurements. *Geoderma* 95, 305-324.

471 Moret-Fernández, D., Latorre, B. 2017. Estimate of the soil water retention curve from  
 472 the sorptivity and  $\beta$  parameter calculated from an upward infiltration experiment.  
 473 *Journal of Hydrology* 544, 352–362.

474 Moret-Fernández, D., Peña-Sancho, C., López, M.V. 2016a. Influence of the wetting  
 475 process on estimation of the water retention curve of tilled soils. *Soil Research*  
 476 doi.org/10.1071/SR15274.

477 Moret-Fernández, D., Latorre, B., Angulo-Martínez, M. 2017a. Comparison of different  
 478 methods to estimate the soil sorptivity from an upward infiltration curve. *Catena*  
 479 155, 86–92.

480 Moret-Fernández, D., Latorre, B., Peña-Sancho, C., Ghezzehei, T.A., 2016b. A  
 481 modified multiple tension upward infiltration method to estimate the soil  
 482 hydraulic properties. *Hydrological Processes*.  
 483 <http://dx.doi.org/10.1002/hyp.10827>.

484 Moret-Fernández, D., Peña-Sancho, C., Latorre, B., Pueyo, Y., López, M.V. 2017b.  
 485 Estimating the van Genuchten retention curve parameters of undisturbed soil from  
 486 a single upward infiltration measurement. *Soil Research*  
 487 doi.org/10.1071/SR16333

488 Moret-Fernández, D., Vicente, J., Latorre, B., Herrero, J., Castañeda, C., López, M.V.,  
 489 2012. TDR pressure cell for monitoring water content retention curves on  
 490 undisturbed soil samples. *Hydrological Processes* 26, 246–254.

491 Peña-Sancho, C., Ghezzehei, T.A., Latorrea, B., Moret-Fernández, D. 2017. Water  
 492 absorption-evaporation method to estimate the soil hydraulic properties.  
 493 *Hydrological Science Journal* 62, 1683-1693.

494 Philip J.R. 1957. The theory of infiltration: 4. Sorptivity and algebraic infiltration  
 495 equations. *Soil Sci.* 84, 257-264.

496 Shao, M., Hudson, R. 1998. Integral method for estimating soil hydraulic properties.  
 497 *Soil Science Society of America Journal* 62, 585-592.

498 Ramos, T., Gonçalves, M., Martins, J., van Genuchten, M.T., Pires, F., 2006. Estimation  
 499 of soil hydraulic properties from numerical inversion of tension disk infiltrometer  
 500 data. *Vadose Zone Journal* 5, 684–696.

501 Rashid, N., Askari, M., Tanaka, T., Simunek, J., van Genuchten, M., Th. 2015. Inverse  
 502 estimation of soil hydraulic properties under oil palm trees. *Geoderma* 241–242,  
 503 306-312

504 RILEM (1980). Essais recommandés pour mesurer l'altération des pierres et évaluer  
 505 l'efficacité des méthodes de traitement. *Matériaux et Constructions*, Bull. RILEM  
 506 13 (75), 175-253.

507 Schumer, M.A., Steiglitz, K. 1968. Adaptive step size random search. *IEEE*  
 508 *Transactions on Automatic Control*. 13, 270-276.

509 Schindler, U. 1980. Ein Schnellverfahren zur Messung der Wasserleitfähigkeit im  
 510 teilgesättigten Boden an Stechzylinderproben. Arch. Acker- Pflanzen- bau  
 511 Bodenk. 24, 1–7.

512 Schindler, U., Müller, L., 2006. Simplifying the evaporation method for quantifying soil  
 513 hydraulic properties. Journal of Plant Nutrition and Soil Science 169, 623–629.

514 Schindler, U., Durner, W., von Unold, G., Müller, L., 2010. Evaporation method for  
 515 measuring unsaturated hydraulic properties of soils: extending the measurement  
 516 range. Soil Science Society of America Journal 74, 1071–1083.

517 Simunek, J., van Genuchten, M.T., 1997. Estimating unsaturated soil hydraulic  
 518 properties from multiple tension disc infiltrometer data. Soil Science 162, 383–  
 519 398.

520 Simunek, J., van Genuchten, M.T., 1996. Estimating unsaturated soil hydraulic  
 521 properties from tension disc infiltrometer data by numerical inversion. Water  
 522 Resources Research. 32, 2683–2696.

523 Simunek, J., Wendroth, O., van Genuchten, M.T., 1998. Parameter estimation analysis  
 524 of the evaporation method for determining soil hydraulic properties. Soil Science  
 525 Society of America Journal 62, 894–895.

526 Solone, R., Bittelli, M., Tomei, F., Morari, F., 2012. Errors in water retention curves  
 527 determined with pressure plates: effects on the soil water balance. Journal of  
 528 Hydrology 470, 65–75.

- 529 van Genuchten, M.T., 1980. A closed form equation for predicting the hydraulic  
530 conductivity of unsaturated soils. Soil Science Society of America Journal 44,  
531 892–898.
- 532 Young, M.H., Karagunduz, A., Siumunek, J., Pennell, K.D., 2002. A modified upward  
533 infiltration method for characterizing soil hydraulic properties. Soil Science  
534 Society of America Journal 66, 57–64.
- 535 Wind, G.P., 1968. Capillary conductivity data estimated by a simple method. In:  
536 Rijtema, P.E., Wassink, H. (Eds.), Water in the unsaturated zone. Vol. 1. Proc.  
537 Wageningen Symp. June 1966. Int. Assoc. Scientific Hydrol. Gentbrugge,  
538 Belgium, pp. 181–191.



## Figures captions

**Figure 1.** Water retention curve and response surfaces for the  $\alpha$ - $n$ ,  $K_s$ - $n$  and  $K_s$ - $\alpha$  planes calculated on a theoretical loam soil for two different initial soil tensions ( $h_i$ ) (Table 1). Contour lines indicate errors of 0.05, 0.1, 0.2, 0.5, 1, 2 and 5 mm, respectively, red line is the contour line for an error of 0.02 mm and blue circle denotes the theoretical value.

**Figure 2.** Simulated cumulative infiltration curves and response surfaces for the  $\alpha$ - $n$ ,  $K_s$ - $n$  and  $K_s$ - $\alpha$  planes calculated for theoretical loamy sand, loam and clay soils (Table 1). Contour lines indicate errors of 0.05, 0.1, 0.2, 0.5, 1, 2 and 5 mm, respectively, red line is the contour line for an error of 0.02 mm and blue circle denotes the theoretical value.

**Figure 3.** Convergence of the optimization to the  $K_s$ ,  $\alpha$  and  $n$  values of a theoretical loam soil from four different initial values.

**Figure 4.** Relationship between the theoretical  $K_s$ ,  $\alpha$  and  $n$  of Table 1 and the corresponding values obtained with the optimization for (a) the best result and (b) the intermediate iteration reaching 0.02 mm error.

**Figure 5.** Experimental relationship between  $S$  (Eq. 4) and  $K_s$ ,  $\alpha$  and  $n$  of the theoretical soils of Table 1.

**Figure 6.** (a) Experimental (circles) and optimized (red line) upward infiltration curve and (b) convergence of  $K_s$ ,  $\alpha$  and  $n$  during the optimization of the experimental sieved clay soil.

**Figure 7.** Relationship between  $K_s$ ,  $\alpha$  and  $n$  estimated on the experimental soils with the Darcy's and PC methods and the corresponding hydraulic values estimated from the inverse analysis (opt) of the upward infiltration curves.

**Figure 8.** Relationship between the sorptivity ( $S$ ) of the experimental soils estimated from Eq.(4) and the optimized  $\alpha$ ,  $n$  and  $K_s$  values and the corresponding sorptivity estimated with Eq.(5) ( $S^*$ ).

Figure 1

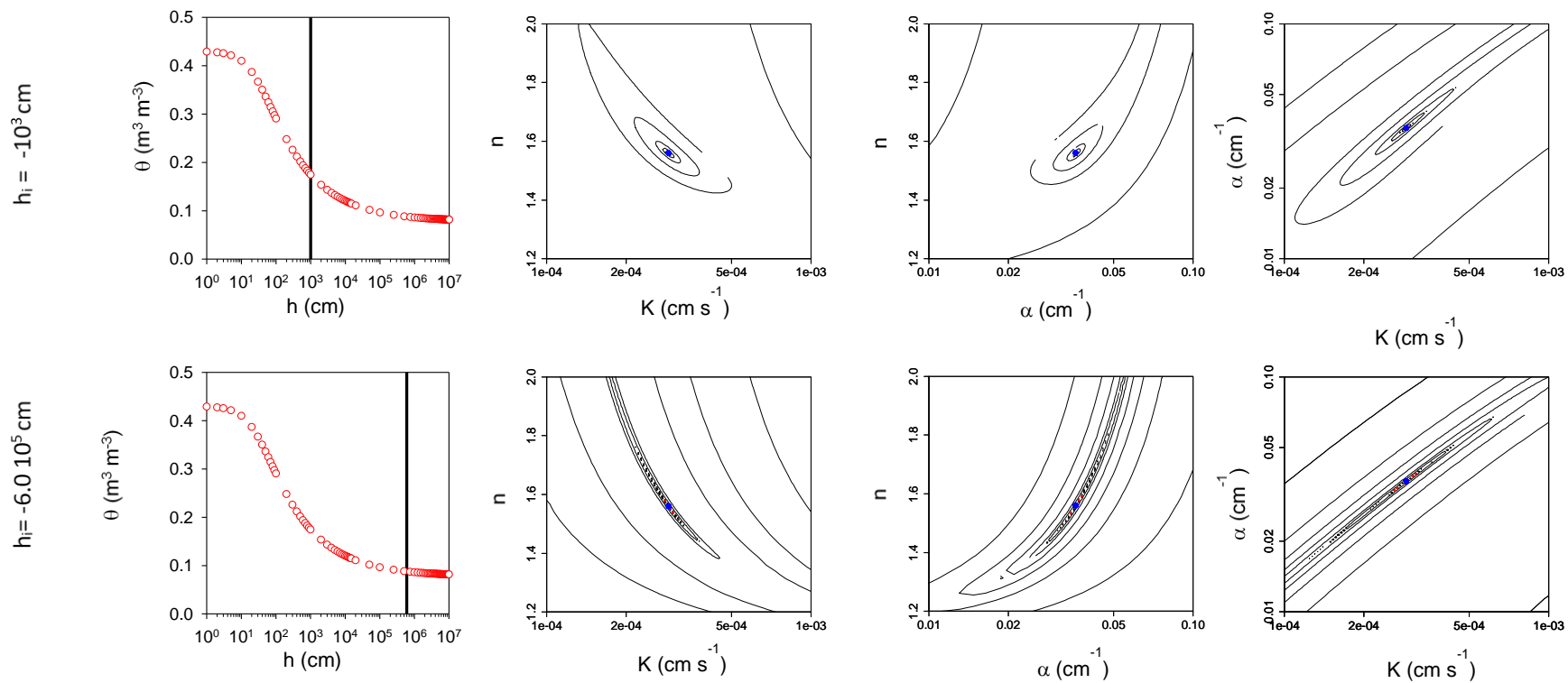


Figure 1.

Figure 2

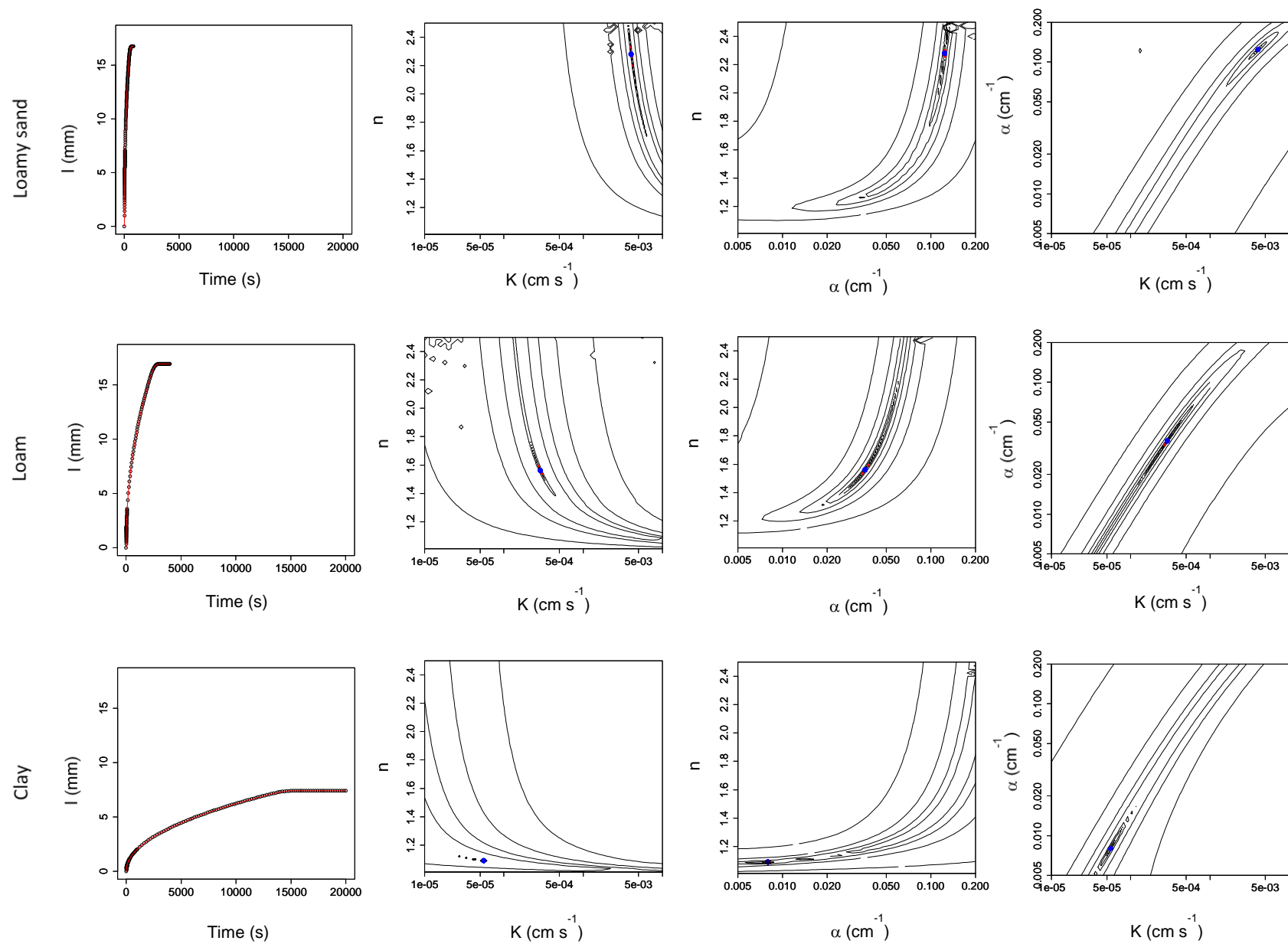


Figure 2.

Figure 3

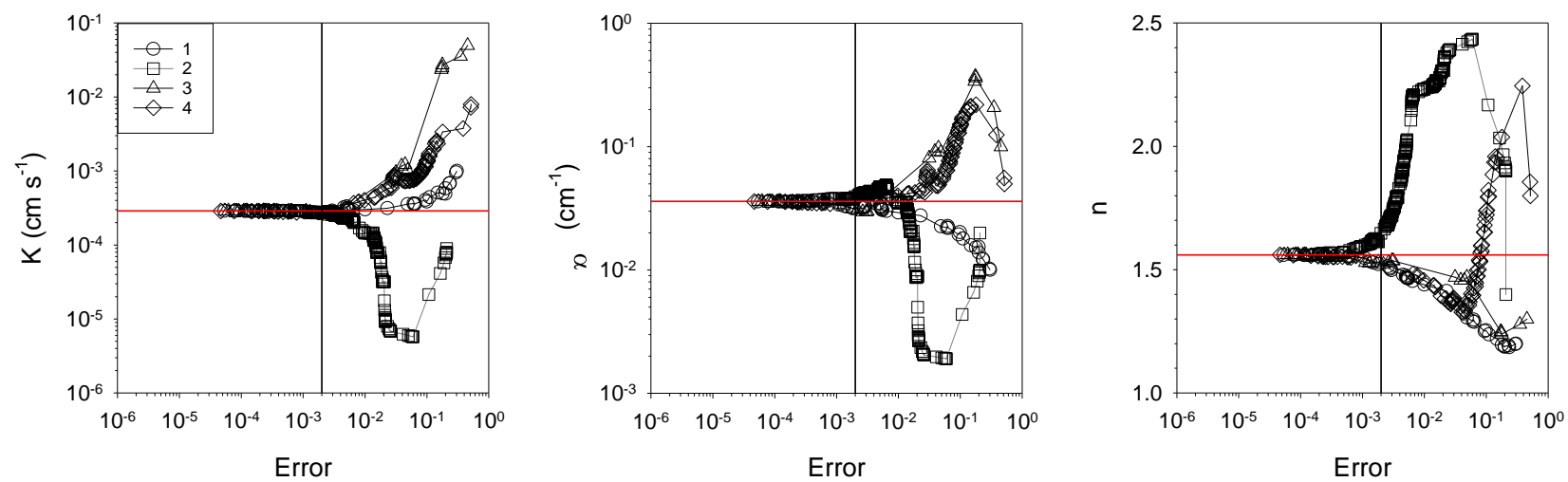


Figure 3.

Figure 4

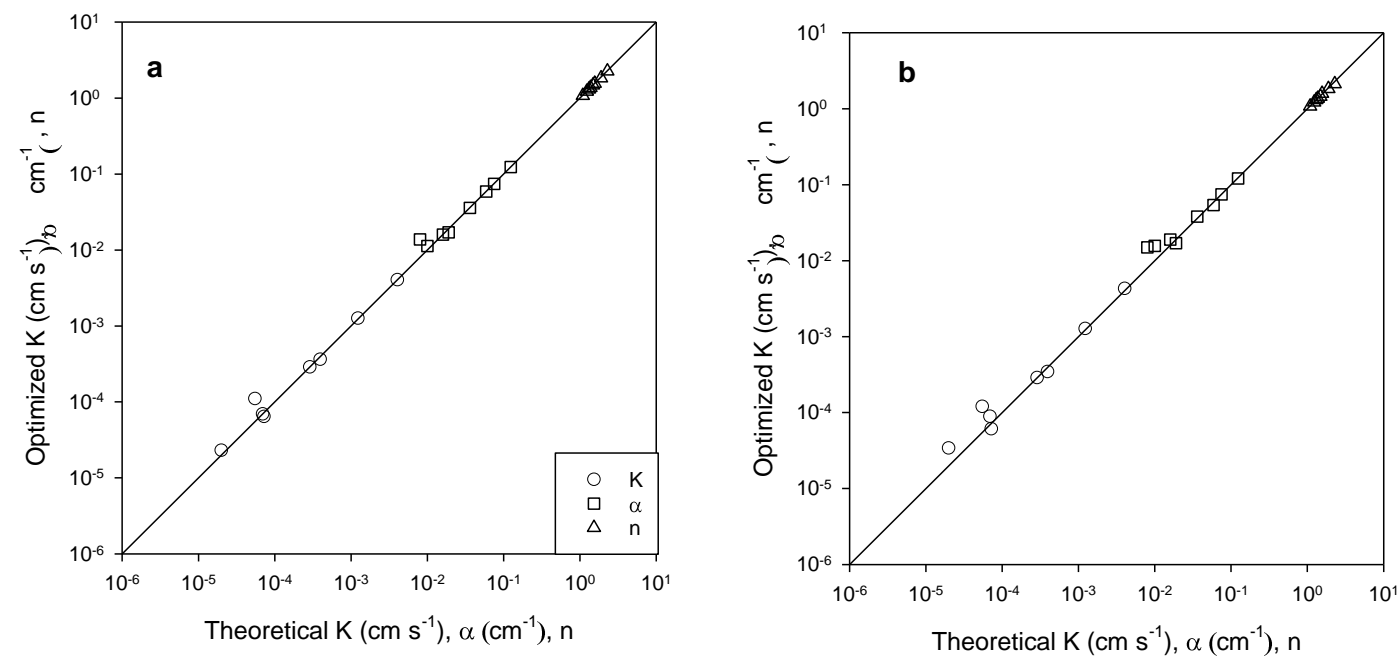


Figure 4

Figure 5

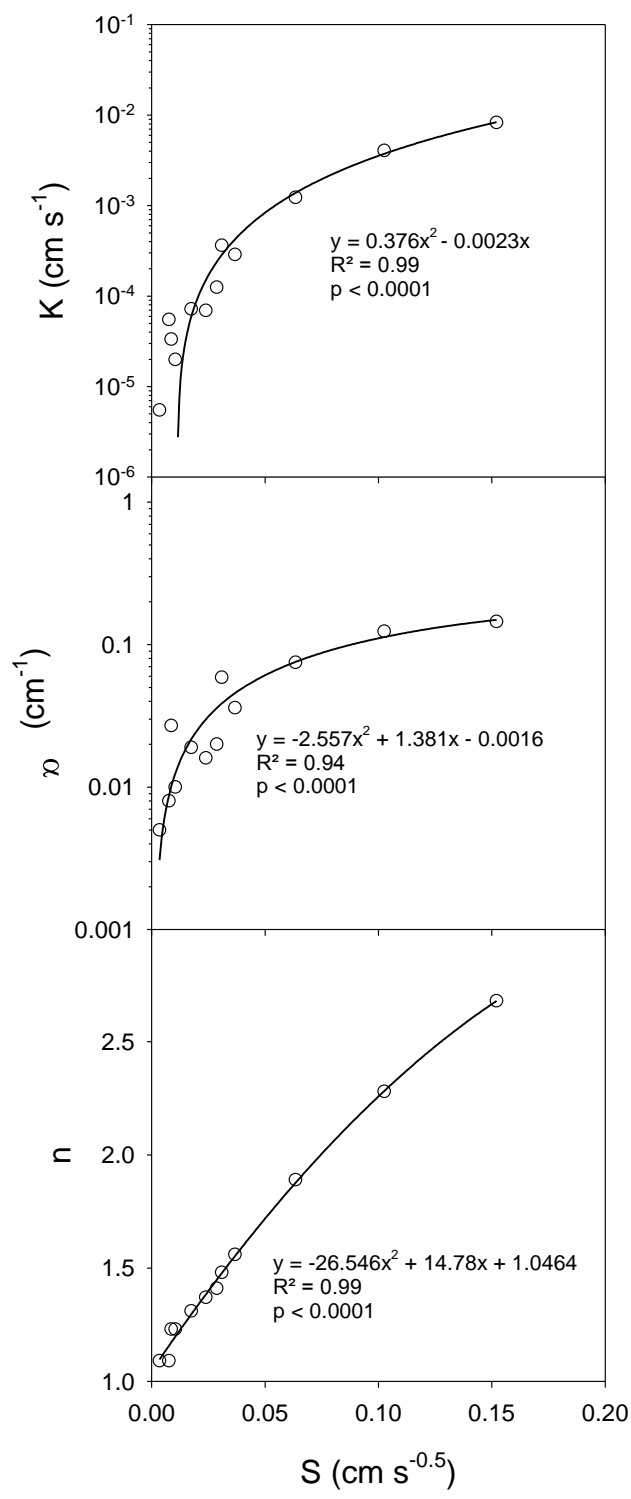


Figure. 5

Figure 6

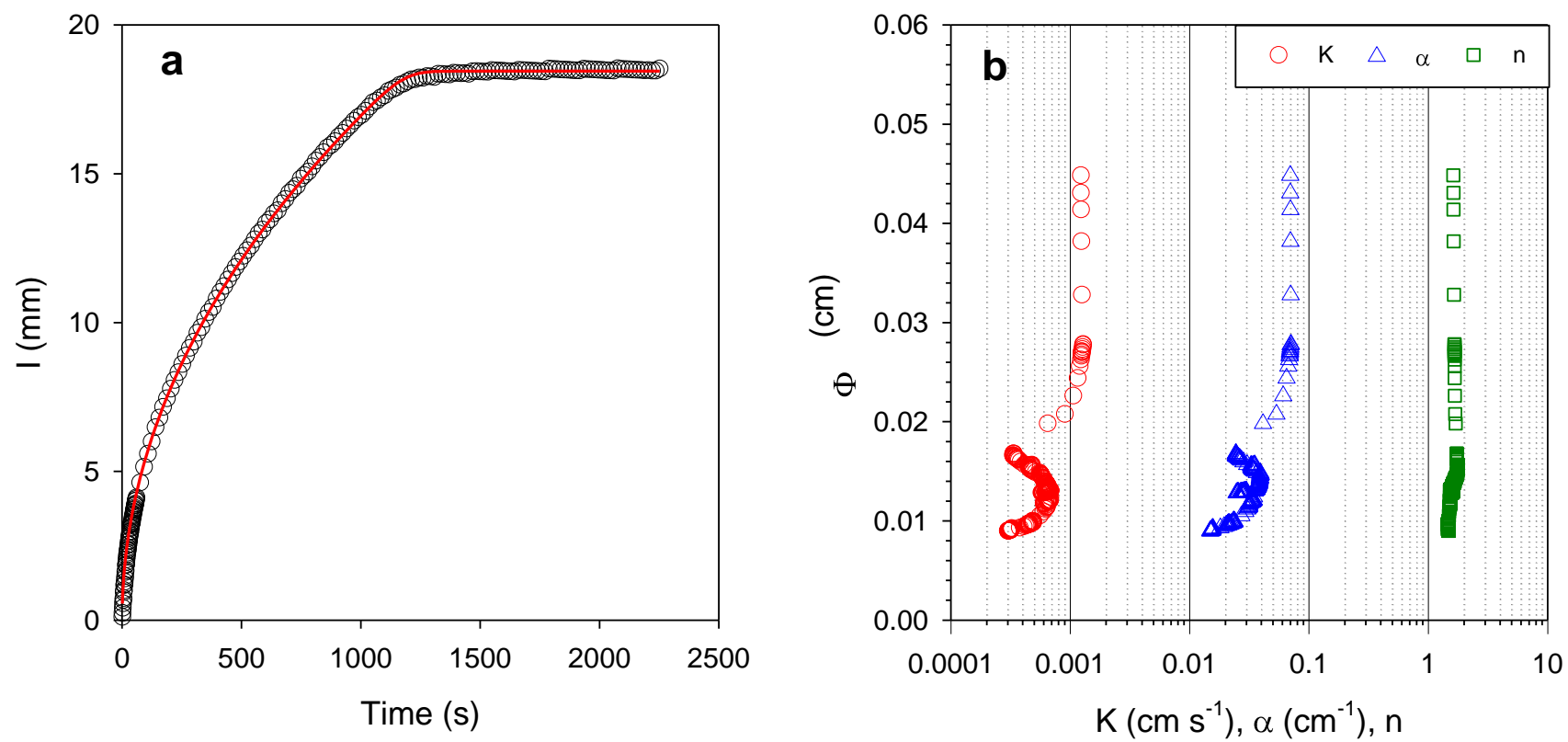


Figure 6.



Figure 7

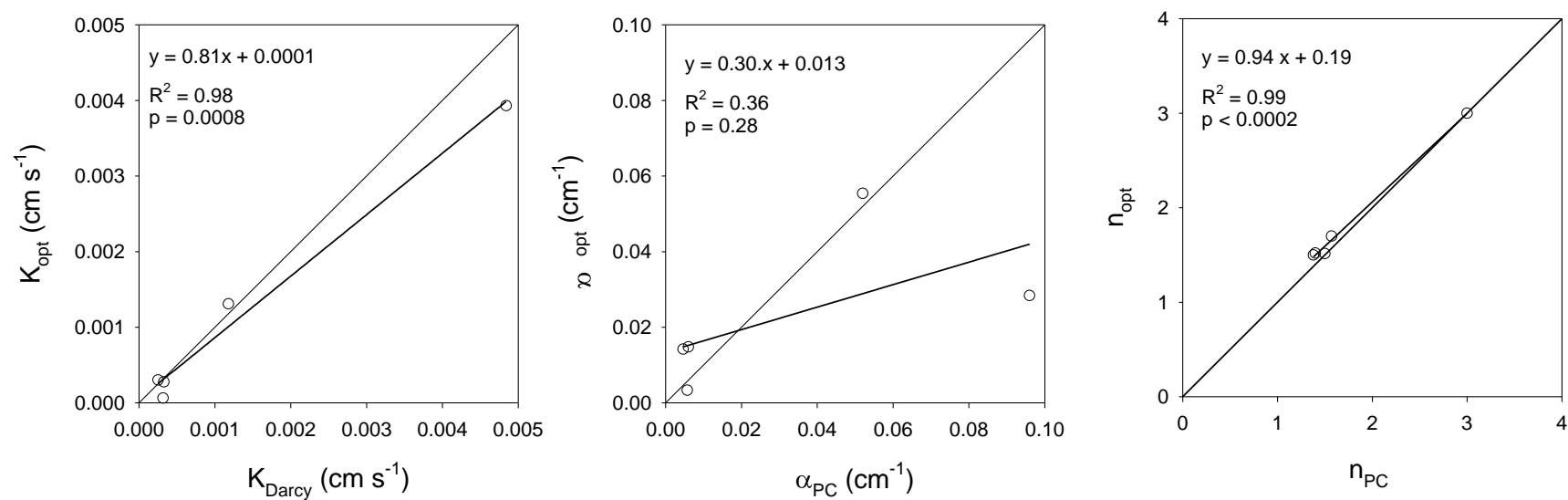


Figure 7.

Figure 8

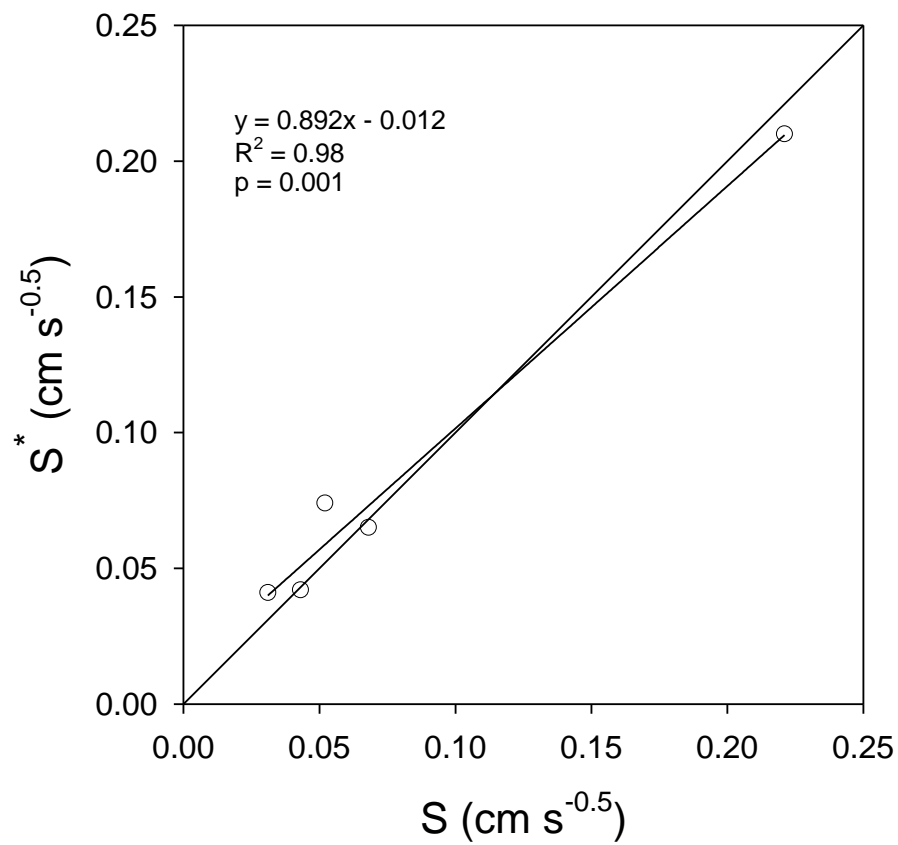


Figure 8.

**Table 1.** Theoretical values of initial ( $\theta_i$ ), saturated ( $\theta_s$ ) and residual ( $\theta_r$ ) water content,  $\alpha$  and  $n$  parameters of the van Genuchten (1980) water retention curve, saturated hydraulic conductivity ( $K_s$ ), sorptivity calculated with Eq. (4) ( $S$ ) and estimated from Eq. (5) ( $S^*$ ), and  $K_s$ ,  $\alpha$  and  $n$  parameters ( $K_s'$ ,  $\alpha'$  and  $n'$ ) estimated from  $K_s(S)$ ,  $\alpha(S)$  and  $n(S)$  relationships (Fig. 3).

	$\theta_i$	$\theta_r$	$\theta_s$	$\alpha$	$n$	$K_s$	$S$	$S^*$	$\alpha'$	$n'$	$K_s'$
	cm <sup>3</sup> cm <sup>-3</sup>	cm <sup>3</sup> cm <sup>-3</sup>	cm <sup>3</sup> cm <sup>-3</sup>	cm <sup>-1</sup>		cm s <sup>-1</sup>	cm s <sup>-0.5</sup>		cm <sup>-1</sup>		cm s <sup>-1</sup>
Loamy sand	0.057	0.057	0.41	0.124	2.28	4.05 10 <sup>-3</sup>	0.1025	0.1021	0.106	2.28	3.58 10 <sup>-03</sup>
Sandy loam	0.065	0.065	0.41	0.075	1.89	1.23 10 <sup>-3</sup>	0.0634	0.0635	0.076	1.87	1.42 10 <sup>-03</sup>
Loam	0.079	0.078	0.43	0.036	1.56	2.88 10 <sup>-4</sup>	0.0367	0.0366	0.047	1.55	8.05 10 <sup>-05</sup>
Silt	0.048	0.034	0.46	0.016	1.37	6.93 10 <sup>-5</sup>	0.0238	0.0235	0.031	1.38	1.67 10 <sup>-04</sup>
Sandy clay loam	0.102	0.100	0.39	0.059	1.48	3.64 10 <sup>-4</sup>	0.0309	0.0307	0.036	1.48	2.79 10 <sup>-04</sup>
Clay loam	0.112	0.095	0.41	0.019	1.31	7.22 10 <sup>-5</sup>	0.0174	0.0176	0.022	1.29	7.40 10 <sup>-05</sup>
Silty clay loam	0.135	0.089	0.43	0.010	1.23	1.99 10 <sup>-5</sup>	0.0104	0.0105	0.013	1.19	1.68 10 <sup>-05</sup>
Clay	0.213	0.068	0.38	0.008	1.09	5.55 10 <sup>-5</sup>	0.0076	0.0078	0.009	1.17	3.55 10 <sup>-06</sup>

**Table 2.** Soil particle size, gypsum and organic carbon content, OC, bulk density,  $\rho_b$ , residual,  $\theta_r$ , and saturated,  $\theta_s$ , volumetric water content, saturated hydraulic conductivity,  $K_s'$ ,  $\alpha'$  and  $n'$  calculated from the estimated sorptivity ( $S^*$ ), and error,  $\Phi$  (Eq. 6), obtained by the inverse analysis of the experimental soils

<i>Treatment</i> <sup>*</sup>	<i>Sand</i>	<i>Silt</i>	<i>clay</i>	<i>Gypsum</i>	<i>OC</i>	$\rho_b$	$\theta_r$	$\theta_s$	$S^*$	$K_s'$	$\alpha'$	$n'$	$\Phi$
			g kg <sup>-1</sup>			g cm <sup>-3</sup>	m <sup>3</sup> m <sup>-3</sup>		cm s <sup>-0.5</sup>	cm s <sup>-1</sup>	cm <sup>-1</sup>		mm
<i>Sand</i>	1000	-	-	-	-	1.64	0.02	0.35	0.210	1.65 10 <sup>-2</sup>	0.175	2.97	0.08
<i>Loam</i>	280	470	250	-	11.7	1.25	0.03	0.47	0.074	2.05 10 <sup>-3</sup>	0.086	1.99	0.11
<i>Clay loam</i>	205	497	298	-	19.9	1.33	0.03	0.44	0.065	1.58 10 <sup>-3</sup>	0.077	1.89	0.15
<i>Silt-Gypeseous</i>	316	591	129	703	1.50	1.02	0.01	0.37	0.042	6.61 10 <sup>-4</sup>	0.052	1.62	0.08
<i>Clay</i>	151	344	465	-	12.4	1.30	0.03	0.40	0.041	6.29 10 <sup>-4</sup>	0.051	1.60	0.09

<sup>\*</sup>  $S$  estimated from the inverse analysis of the upward infiltration curve using Eq. (5)